JOURNAL OF COMPUTATIONAL PHYSICS **147,** 337–361 (1998)
ARTICLE NO. CP986092

On the Use of Wavelets in Computational Combustion

R. Prosser and R. S. Cant

CFD Laboratory, University Engineering Department, Trumpington Street, Cambridge CB2 1PZ, United Kingdom
E-mail: rsc10@eng.cam.ac.uk

Received March 27, 1998; revised August 18, 1998

The numerical simulation of combustion remains a challenging task. Flames are often thin and occupy a relatively small volume within the domain of interest. Nevertheless all of the combustion chemistry and much of the associated molecular transport takes place within the flame itself, giving rise to a structure that must be resolved if the simulated flame response is to be captured accurately. The present work examines the use of a wavelet-based method in this context. A spatial discretisation scheme using biorthogonal wavelets is presented and is applied to a test problem involving flame propagation in a representative fuel–air mixture, in which the chemistry is treated using a standard four-step reduced reaction mechanism. A novel and elegant boundary treatment is adopted in the wavelet scheme to enable the implementation of physically realistic boundary conditions. Results show that the wavelet scheme is stable and accurate and, moreover, is able to exploit the natural data-compression properties of wavelets to represent the solution using a fraction of the storage required for more conventional methods.

Key Words: turbulent combustion.

1. INTRODUCTION

Direct numerical simulation (DNS) of turbulent flows is an activity severely limited by presently available computer power. It has long been known (e.g. Corrsin [1]) that, in order to resolve accurately the governing Navier–Stokes equations, the number of computational cells scales as a super-linear power of the Reynolds number. Reacting systems add additional complexity to this already bleak picture. In many flows of industrial interest, the length and time scales associated with the reaction mechanism are much smaller than those of the fluid turbulence, and the resolution requirements for chemically active flow simulations are thereby considerably increased. When this is added to the computational expense incurred by the stiffness of highly nonlinear reaction rate source terms, it appears that reacting flow

0021-9991/98 $25.00

simulations of significant complexity will remain firmly out of reach for the foreseeable future. Nonetheless, the same spatial and temporal stiffness that gives rise to such demanding computations may paradoxically provide a foothold for efficient numerical methods. Many industrial processes involving combustion occupy the *laminar flamelet regime* [2, 3], where the turbulent flame can be regarded as a highly localised sheet of chemical activity, either side of which the fluid composition remains relatively constant.

The ability of wavelet-based methods to analyse functions in terms of their *local* rates of change appears eminently suited to the numerical investigation of nonlinear partial differential equations, the solutions to which often contain a large number of disparate length scales. In particular, the efficient discretisation of fluid flow problems has been the focus of a number of recent investigations, both with chemical reaction [4–6] and without [7–9]. Many of the discretisations proposed to date have been limited to periodic domains, although recent efforts have led to advances in nonperiodic discretisations [10–12].

In this paper, we propose a wavelet-based scheme intended for combustion problems which adopts a collocation strategy. In traditional collocation methods, the solution to the set of governing equations is obtained on a grid of collocation points located in the physical domain. In contrast, we compute the solution to the set of *wavelet transformed* equations on grids of collocation points located in the transform domains. The solution is only returned to the physical space in order to evaluate nonlinear inertial and chemical reaction rate terms. The advantage of this approach is that, while the solution is expressed in terms of the wavelet spaces, it is possible to exploit its sparsity in order to reduce the amount of storage required to resolve the chemistry fields.

Section 2 reviews the physical aspects of the problem, Section 3 revisits some topics from multiresolution analysis and, in particular, biorthogonal wavelet systems. Section 4 discusses the strategy adopted and the incorporation of boundary conditions. Section 5 examines results obtained using the proposed scheme while Section 6 presents further discussion and conclusions.

2. THE PROBLEM

To demonstrate the proposed wavelet discretisation, the reacting Navier–Stokes equations will be investigated. In the most general three-dimensional setting, there are $N + 5$ coupled equations which between them describe the time-dependent evolution of density, velocity, energy, and N reacting species. Realistic treatment of chemical reaction mechanisms usually requires many hundreds of elemental steps involving a similarly large number of reaction intermediaries [13]. When we add to this complexity the three-dimensional nature of turbulence, it quickly becomes clear that a full treatment of general reacting flows presents a challenge beyond the capabilities of presently available computer power. Simplifications to the general case usually take the form of a restricted problem definition and/or a simpler treatment of the reaction kinetics.

The most extreme simplification that can be made to the reaction mechanism is to reduce the chemical kinetics to an irreversible single step mechanism of the form

$$\text{Reactants} \rightarrow \text{Products}.$$

This mechanism is governed by an Arrhenius rate law, and at any point in the flow the thermochemical state of the fluid is given by a scalar c, referred to as a *reaction progress variable*

[3, 14–16]. Asymptotic analyses of such simplified systems [17–19] reveal that there predominantly exist two scales in the flow: one associated with the convective–diffusive part of the flame, and one related to the reactive–diffusive part.

In a realistic reacting flow, the spatial stiffness of the chemical mechanism introduces a considerable range of length scales existing simultaneously in the flame structure. Ideally then, we wish to examine our wavelet-based scheme's capacity to deal with multiple length scales appearing in localised regions of the computational domain. With this goal in mind, the mechanism we have adopted is that of a premixed methane–air flame with the chemistry described by a four-step reduced reaction mechanism. While the discretisation discussed here is one-dimensional, the techniques we have developed remain quite general and can be applied in a straightforward manner to multidimensional problems via the use of tensor products of the one-dimensional basis functions. A forthcoming paper will detail the application of the method to fully three-dimensional DNS investigations of reduced chemistry methane–air systems.

2.1. *Governing Equations*

Starting from the nonreacting Navier–Stokes equations as detailed in [20] and supplementing these with the equations for species transport [17], the reacting Navier–Stokes system can be expressed as

$$\begin{aligned}
\frac{\partial}{\partial t}(\rho) + \frac{\partial}{\partial x_k}(\rho u_k) &= 0 \\
\frac{\partial}{\partial t}(\rho u_i) + \frac{\partial}{\partial x_k}(\rho u_i u_k) &= -\frac{\partial P}{\partial x_i} + \frac{\partial}{\partial x_k}(\tau_{ik}) \\
\frac{\partial}{\partial t}(\rho E) + \frac{\partial}{\partial x_k}(\rho u_k E) &= -\frac{\partial}{\partial x_k}(P u_k) + \frac{\partial}{\partial x_k}(u_i \tau_{ki}) - \frac{\partial q_k}{\partial x_k} \\
\frac{\partial}{\partial t}(\rho Y_\alpha) + \frac{\partial}{\partial x_k}(\rho u_k Y_\alpha) &= w_\alpha + \frac{\partial}{\partial x_k}\left\{ \rho \mathcal{D}_\alpha \frac{\partial Y_\alpha}{\partial x_k} \right\}.
\end{aligned} \tag{1}$$

In the above system of equations E is the *stagnation* internal energy and is defined as [20]

$$E = h - RT + \frac{u^2}{2},$$

where h, the enthalpy, is given by [17]

$$h = \sum_\alpha h_\alpha Y_\alpha = \sum_\alpha Y_\alpha \left\{ \Delta h_\alpha^0 + \int_{T_0}^{T} c_{p\alpha}(T')\, dT' \right\}. \tag{2}$$

Δh_α^0 is the enthalpy of formation of species α at reference temperature T_0. The temperature dependence of $c_{p\alpha}$ for each species was taken from the CHEMKIN thermodynamic database [21]. The heat flux vector q_k is defined as [17]

$$q_k = -\lambda \frac{\partial T}{\partial x_k} + \rho \sum_{\alpha=1}^{N} h_\alpha Y_\alpha V_{\alpha k}, \tag{3}$$

wherein the assumption has been made that the contributions arising from radiation, thermal diffusion, and concentration gradients are negligible. The system is closed by the inclusion of the thermal equation of state,

$$P = \rho R T,$$

where R refers to the characteristic gas constant for the mixture.

If the diffusion velocities V_α are modelled in terms of Fick's diffusion hypothesis [22], then substitution of this approximation into the one-dimensional form of equation set (1) and subsequent nondimensionalisation leads to

$$\begin{aligned}
\frac{\partial}{\partial t}(\rho) + \frac{\partial}{\partial x}(\rho u) &= 0 \\
\frac{\partial}{\partial t}(\rho u) + \frac{\partial}{\partial x}(\rho u u) &= -\frac{\partial P}{\partial x} + \frac{4}{3\mathrm{Re}}\frac{\partial}{\partial x}\left(\mu \frac{\partial u}{\partial x}\right) \\
\frac{\partial}{\partial t}(\rho E) + \frac{\partial}{\partial x}(\rho u E) &= -(\gamma-1)\mathcal{M}^2 \frac{\partial}{\partial x}(P u) + \frac{1}{\mathrm{Re}\,\mathrm{Pr}}\frac{\partial}{\partial x}\left\{\lambda \frac{\partial T}{\partial x}\right\} \\
&\quad + \frac{1}{\mathrm{Re}\,\mathrm{Sc}}\sum_{\alpha=1}^{N}\frac{\partial}{\partial x}\left\{\rho h_\alpha \mathcal{D}_{\alpha\beta}\frac{\partial Y_\alpha}{\partial x}\right\} \\
&\quad + \frac{4(\gamma-1)\mathcal{M}^2}{3\mathrm{Re}}\frac{\partial}{\partial x}\left(\mu u \frac{\partial u}{\partial x}\right) \\
\frac{\partial}{\partial t}(\rho Y_\alpha) + \frac{\partial}{\partial x}(\rho u Y_\alpha) &= w_\alpha + \frac{1}{\mathrm{Re}\,\mathrm{Sc}}\frac{\partial}{\partial x}\left\{\rho \mathcal{D}_{\alpha\beta}\frac{\partial Y_\alpha}{\partial x}\right\}.
\end{aligned} \tag{4}$$

In this last set of equations, the following dimensionless groups have been employed

$$\mathrm{Re} = \frac{\rho_0 u_0^l l_0}{\mu_0}, \quad \mathrm{Pr} = \frac{\mu_0 (c_p)_0}{\lambda_0}, \quad \mathrm{Sc} = \frac{\mu_0}{(\rho\mathcal{D})_0}$$

$$\mathcal{M}^2 = \frac{\left(u_0^l\right)^2}{\gamma_0 R_0 T_0}, \quad \gamma_0 = \frac{(c_p)_0}{(c_v)_0}.$$

The transport equations are closed through the dimensionless forms of the caloric and thermal equations of state:

$$\begin{aligned}
E &= h - RT + \frac{(\gamma-1)\mathcal{M}^2}{2}u^2 \\
P &= \frac{\rho T}{(\gamma-1)\mathcal{M}^2}\sum_\alpha R_\alpha Y_\alpha.
\end{aligned} \tag{5}$$

2.2. *Reaction Mechanism*

The reaction mechanism adopted is that discussed in the asymptotic analysis of Peters and Williams [23] and consists of the following steps:

$$\begin{aligned}
&\text{I.} && \mathrm{CH_4 + 2H + H_2O \rightarrow CO + 4H_2} \\
&\text{II.} && \mathrm{CO + H_2O \rightleftharpoons CO_2 + H_2} \\
&\text{III.} && \mathrm{2H + M \rightarrow H_2 + M} \\
&\text{IV.} && \mathrm{O_2 + 3H_2 \rightleftharpoons 2H_2O + 2H.}
\end{aligned} \tag{6}$$

The associated reaction rates for each of the species involved are

$$\begin{aligned} w_{CH_4} &= W_{CH_4}(-\bar{w}_I) \\ w_{CO} &= W_{CO}(\bar{w}_I - \bar{w}_{II}) \\ w_{CO_2} &= W_{CO_2}(\bar{w}_{II}) \\ w_H &= 2W_H(-\bar{w}_I - \bar{w}_{III} + \bar{w}_{IV}) \\ w_{H_2} &= W_{H_2}(4\bar{w}_I + \bar{w}_{II} + \bar{w}_{III} - 3\bar{w}_{IV}) \\ w_{H_2O} &= W_{H_2O}(-\bar{w}_I - \bar{w}_{II} + 2\bar{w}_{IV}) \\ w_{O_2} &= W_{O_2}(-\bar{w}_{IV}) \\ w_{N_2} &= 0, \end{aligned} \tag{7}$$

where W_α are the molar masses of each species, and the *molar* reaction rates $\bar{w}_I, \bar{w}_{II}, \bar{w}_{III}$, and $\bar{w}_{IV}$ are given by

$$\begin{aligned} \bar{w}_I &= k_{11}[\mathrm{CH_4}][\mathrm{H}] \\ \bar{w}_{II} &= \frac{k_{10}}{K_3}\frac{[\mathrm{H}]}{[\mathrm{H_2}]}\left\{[\mathrm{CO}][\mathrm{H_2O}] - \frac{[\mathrm{CO_2}][\mathrm{H_2}]}{K_{II}}\right\} \\ \bar{w}_{III} &= k_5[\mathrm{O_2}][\mathrm{H}][\mathrm{M}] \\ \bar{w}_{IV} &= k_1[\mathrm{H}]\left\{[\mathrm{O_2}] - \frac{[\mathrm{H}]^2[\mathrm{H_2O}]^2}{[\mathrm{H_2}]^3 K_{IV}}\right\}. \end{aligned} \tag{8}$$

Each of the rate constants can be calculated using the general Arrhenius form

$$k_n = B_n T_{\alpha_n} \exp\left\{\frac{-E_n}{\mathcal{R}^0 T}\right\} \tag{9}$$

and the equilibrium constants K_3, K_{II}, and K_{IV} can be calculated from

$$\begin{aligned} K_3 &= \frac{[\mathrm{H}][\mathrm{H_2O}]}{[\mathrm{H_2}][\mathrm{OH}]} = C_3 \exp\left\{\frac{T_3}{T}\right\} \\ K_{II} &= \frac{[\mathrm{CO_2}][\mathrm{H_2}]}{[\mathrm{CO}][\mathrm{H_2O}]} = C_{II} \exp\left\{\frac{T_{II}}{T}\right\} \\ K_{IV} &= \frac{[\mathrm{H}]^2[\mathrm{H_2O}]^2}{[\mathrm{H_2}]^3[\mathrm{O_2}]} = C_{IV} \exp\left\{\frac{T_{IV}}{T}\right\}, \end{aligned} \tag{10}$$

where C_3, C_{II}, and C_{IV} are dimensionless constants. The numbering of the reaction steps and the values of the various rate parameters are the same as those given in [23].

Molecular transport properties are calculated using two assumptions. First, we follow Echekki and Chen [24] in relating the thermal conductivity to the specific heat of the mixture via the relation

$$\frac{\lambda}{c_p} = A\left\{\frac{T}{T_r}\right\}^{0.7}, \tag{11}$$

where A is a constant ($=2.58 \times 10^{-5}$ kg/ms), and T_r is a reference temperature ($=300$ K). Second, we assume that the Prandtl and Lewis numbers, defined as

$$\mathrm{Pr} = \frac{\mu c_p}{\lambda}, \quad \mathrm{Le}_\alpha = \frac{\lambda}{\rho \mathcal{D}_\alpha c_p},$$

remain constant. Assuming a fixed Prandtl number then gives a relationship for the temperature dependence of the viscosity. Fixed Lewis numbers similarly provide temperature dependencies for the mass diffusivities of each of the species. All of the parameters used during this study are detailed in Section 5.

3. CLASSICAL BIORTHOGONAL WAVELET BASES

Biorthogonal wavelet systems are derived from a paired hierarchy of approximation subspaces,

$$\begin{aligned} \mathbf{V}_{J-1} \subset \mathbf{V}_J \subset \mathbf{V}_{J+1} \ldots \\ \tilde{\mathbf{V}}_{J-1} \subset \tilde{\mathbf{V}}_J \subset \tilde{\mathbf{V}}_{J+1} \ldots . \end{aligned} \tag{12}$$

The basis functions for these spaces are the *primal* scaling function $\phi(x)$ and the *dual* scaling function $\tilde{\phi}(x)$. Biorthogonality is enforced by first defining two *innovation* spaces $\mathbf{W}_J$ and $\tilde{\mathbf{W}}_J$ such that

$$\begin{aligned} \mathbf{V}_{J+1} &= \mathbf{V}_J \oplus \mathbf{W}_J \\ \tilde{\mathbf{V}}_{J+1} &= \tilde{\mathbf{V}}_J \oplus \tilde{\mathbf{W}}_J, \end{aligned} \tag{13}$$

with the further requirement [25]

$$\tilde{\mathbf{V}}_J \perp \mathbf{W}_J, \quad \mathbf{V}_J \perp \tilde{\mathbf{W}}_J. \tag{14}$$

The innovation spaces so defined verify

$$\bigoplus_{i=-\infty}^{\infty} \mathbf{W}_i = L^2(\mathbb{R}) = \bigoplus_{i=-\infty}^{\infty} \tilde{\mathbf{W}}_i \tag{15}$$

The basis functions for the innovation spaces are the primal and dual wavelets $\psi(x)$ and $\tilde{\psi}(x)$, respectively. In the classical biorthogonal setting, the primal and dual basis functions each satisfy a two-scale relation

$$\begin{aligned} \phi(x) &= \sqrt{2} \sum_{m \in \mathbb{Z}} h_m \phi(2x - m), \quad \psi(x) = \sqrt{2} \sum_{m \in \mathbb{Z}} g_m \phi(2x - m) \\ \tilde{\phi}(x) &= \sqrt{2} \sum_{m \in \mathbb{Z}} \tilde{h}_m \tilde{\phi}(2x - m), \quad \tilde{\psi}(x) = \sqrt{2} \sum_{m \in \mathbb{Z}} \tilde{g}_m \tilde{\phi}(2x - m). \end{aligned} \tag{16}$$

Each of the two scale relations appearing in Eq. (16) makes use of an appropriately defined *quadrature mirror filter*—defined in terms of the sets of coefficients h_m, g_m, $\tilde{h}_m$, and $\tilde{g}_m$—which together uniquely define all of the properties associated with the basis functions. If the biorthogonal system has compact support, then this feature is reflected in the limited number of nonzero coefficients defining the quadrature mirror filters.

The projection of a function $f(x)$ onto a finite-dimensional scaling function space $\mathbf{V}_J$, or a similarly finite-dimensional wavelet space $\mathbf{W}_J$, is accomplished in a way similar to the algorithm described for orthogonal systems,

$$\begin{aligned} P_{\mathbf{V}_J}\{f(x)\} &= \sum_{k\in\mathbb{Z}} \langle f(u), \tilde{\phi}_{J,k}(u)\rangle\, \phi_{J,k}(x) \\ P_{\mathbf{W}_J}\{f(x)\} &= \sum_{k\in\mathbb{Z}} \langle f(u), \tilde{\psi}_{J,k}(u)\rangle\, \psi_{J,k}(x), \end{aligned} \tag{17}$$

in which $\langle \cdot, \cdot \rangle$ represents an inner product. Equations (17) are used in conjunction with Eqs. (16) and (13) to provide a framework of a fast wavelet transform:

$$\begin{aligned} \langle f, \tilde{\phi}_{J,k}\rangle = S^f_{J,k} &= \sum_m \tilde{h}_m S^f_{J+1,m+2k} \\ \langle f, \tilde{\psi}_{J,k}\rangle = d^f_{J,k} &= \sum_m \tilde{g}_m S^f_{J+1,m+2k} \\ S^f_{J+1,k} &= \sum_\xi \left\{ h_{k-2\xi} S^f_{J,\xi} + g_{k-2\xi} d^f_{J,\xi} \right\}. \end{aligned} \tag{18}$$

The principal difference in using biorthogonal systems lies in the fact that the analysis filters used for decomposing a signal are different from the synthesis filters used to reconstruct it [25].

3.1. *Nonperiodic Discretisations: Motivation*

During combustion simulations, periodic boundary conditions introduce considerable restrictions when realistic heat release rates are encountered. In such cases it is impossible to obtain quasi-steady solutions as all state and hydrodynamic quantities vary strongly with time. To obtain quasi-steady solutions of greater practical value, a nonperiodic discretisation must be sought which allows the low density, high temperature burnt products to be convected out of the domain. There currently exists a number of constructions able to discretise problems defined on nonperiodic domains. Cohen, Daubechies, and Vial [26] provide a basis consisting of three sets of wavelets; one set for each edge of the domain and one set of "internal" wavelets. Their construction is completed by employing matrices at each end of the transform vector to ensure that polynomial sequences across all scales are mapped to zero under the action of the wavelet filters. Monasse and Perrier [27] also provide a construction using compactly supported orthogonal wavelets. In their construction, however, they do not use a staggered support for the construction of the edge wavelets. Edge effects are incorporated through the use of an approximate projection quadrature. The distribution of errors associated with the quadrature is nonuniform and the scheme appears unsuitable for combustion problems [28].

Cai *et al*. develop an interval-based construction based on spline wavelets [29, 30], which they subsequently employ in an adaptive manner to resolve a two-dimensional reaction–diffusion equation. A spatially adaptive algorithm also provides the motivation for the scheme discussed by Vasiliev *et al*. [10–12]. In this approach, the construction of edge wavelets is avoided by extending the solution to the governing equations beyond the immediate domain of interest. The boundary conditions and evaluations of nonlinear terms are then applied in the physical domain, wherein the solution is also time advanced.

With the exception of [10–12], most of the schemes discussed do not readily deal with the kind of sophisticated boundary conditions with which we have to contend. In order to accommodate these general boundary conditions, we propose a scheme which makes use of *second generation wavelets*.

The term "second generation"—coined by Sweldens *et al*. [31–33]—is used to refer to the fact that the manner in which such wavelets are designed is more general than classical ("first generation") techniques. The resultant basis functions are biorthogonal, and can be derived for a multiplicity of discretisations, including those with uneven grid spacing and domains defined on manifolds. From this class of basis functions, we have adopted the *interpolating* wavelet family discussed by Donoho [34]. The basis functions take the forms

$$\begin{aligned} \phi_{j,k}(x) &= \phi(2^j x - k) \\ \psi_{j,k}(x) &= \phi(2^{j+1}x - 2k - 1) \\ \tilde{\phi}_{j,k}(x) &= \delta(x - x_{j,k}), \end{aligned} \tag{19}$$

where $\delta(\cdot)$ is the Dirac delta function. An explicit relation describing the dual wavelet is unknown. The absence of a $\sqrt{2}$ multiple in the previous definitions reflects the fact that we have adopted an $\|\cdot\|_\infty$ norm, in preference to the more usual $\|\cdot\|_2$ norm. The choice of normalisation is based on the recommendations of Donoho [34] and reduces the complexity of the resulting calculations.

The basis is said to be *interpolating* in the sense that $\phi(x) = \psi(2x - 1)$ satisfies

$$\phi(k) = \begin{cases} 1, & k = 0, \\ 0, & k \neq 0, k \in \mathbb{Z}. \end{cases} \tag{20}$$

3.2. *Fast Transform Algorithm*

The projection of a function $f(x)$ onto a finite-dimensional scaling function space $\mathbf{V}_J$ is defined here as

$$\begin{aligned} P_{\mathbf{V}_J}\{f(x)\} &= \sum_{k\in\mathbb{Z}} \langle f(u), \tilde{\phi}_{J,k}(u)\rangle \phi_{J,k}(x) \\ &= \sum_{k\in\mathbb{Z}} f\left\{\frac{k}{2^J}\right\} \phi_{J,k}(x) \\ &= \sum_{k\in\mathbb{Z}} S^f_{J,k}\phi_{J,k}(x), \end{aligned} \tag{21}$$

where $S^f_{J,k} = f\{k/2^J\}$ has been introduced in order to maintain consistency with existing literature. A possible drawback arises with this set of basis functions in that the wavelet coefficients cannot be calculated using classical (i.e. filter-based) techniques, as the form for the dual wavelet is unknown. Instead, the coefficients must be derived directly from Eq. (13):

$$\begin{aligned} P_{\mathbf{W}_j}\{f(x)\} &= P_{\mathbf{V}_{j+1}}\{f(x)\} - P_{\mathbf{V}_j}\{f(x)\} \\ \sum_{l\in\mathbb{Z}} d^f_{j,l}\psi_{j,l}(x) &= \sum_{m\in\mathbb{Z}} S^f_{j+1,m}\phi_{j+1,m}(x) - \sum_{n\in\mathbb{Z}} S^f_{j,n}\phi_{j,n}(x). \end{aligned} \tag{22}$$

Using the notation of Eqs. (19) and (20), it is straightforward to show that an arbitrary wavelet coefficient $d^f_{j,m}$ can be calculated from

$$\begin{aligned} d^f_{j,m} &= S^f_{j+1,2m+1} - \sum_{n\in\mathbb{Z}} S^f_{j,n}\phi\left\{m-n+\frac{1}{2}\right\} \\ &= S^f_{j+1,2m+1} - \sum_{n\in\mathbb{Z}} \Gamma_{mn} S^f_{j,n}, \end{aligned} \tag{23}$$

where Γ_{mn} is a square matrix of size $2^j \times 2^j$ for periodic discretisations or $(2^j+1)\times(2^j+1)$ for nonperiodic domains (the reason for the difference in the matrix' size will be discussed shortly):

$$\Gamma_{mn} = \phi\left\{m-n+\frac{1}{2}\right\}.$$

Due to the compact support of the primal scaling function, this matrix has a band-diagonal structure.

In the discussion presented by Donoho [34], the primal scaling function is taken to be one of the family of *fundamental solutions* derived by Deslauriers and Dubuc [35]. Each primal scaling function then satisfies a two-scale relation:

$$\phi(x) = \sum_{\xi\in\mathbb{Z}} \phi\left\{\frac{\xi}{2}\right\}\phi(2x-\xi). \tag{24}$$

The functions $\phi(x)$ have compact support and it follows that the summation appearing in Eq. (24) is finite in extent. We note in passing that rigorous estimates for the continuity of the fundamental solution exist and can be related to its polynomial span N [33]. The values of $\phi(\xi/2)$ can also be calculated from an explicit relation [33]:

$$\phi\left\{k+\frac{1}{2}\right\} = (-1)^{N/2+k}\frac{\prod_{i=0}^{N-1}\left(i-\frac{N-1}{2}\right)}{\left(k+\frac{1}{2}\right)\left(\frac{N}{2}+k\right)!\left(\frac{N}{2}-k-1\right)!}, \quad k=-N,\ldots,N-1. \tag{25}$$

The transform algorithm is completed by recalling that the definition of the dual scaling function leads to the following causal relation for the scaling function coefficients in the approximation space $\mathbf{V}_j$:

$$\begin{aligned} S^f_{j,k} &= \langle f(u), \delta(u-u_{j,k})\rangle \\ &= \langle f(u), \delta(u-u_{j+1,2k})\rangle = S^f_{j+1,2k}. \end{aligned} \tag{26}$$

Regardless of the choice of primal scaling function, the *transform vector* which arises from the wavelet transform will have a structure similar to that shown below:

$$\begin{array}{l} \left\{S^f_{J,0}\ S^f_{J,1}\ S^f_{J,2}\ \cdots \right. \qquad\qquad\qquad\qquad \left. \cdots\ S^f_{J,2^J(-1)}\right\}^{\mathrm{T}} \\ \qquad\qquad\qquad\qquad\qquad\qquad \downarrow \\ \left\{d^f_{J-1,0}\ d^f_{J-1,1}\ \cdots\ d^f_{J-1,2^{J-1}-1}\right. \quad \left|S^f_{J-1,0}\ S^f_{J-1,1}\ \cdots \right. \qquad \left. S^f_{J-1,2^{J-1}(-1)}\right\}^{\mathrm{T}} \\ \qquad\qquad\qquad\qquad\qquad\qquad \downarrow \\ \left\{d^f_{J-1,0}\ \cdots\ d^f_{J-1,2^{J-1}-1}\right| d^f_{J-2,0} \quad \cdots\ d^f_{J-2,2^{J-2}-1}\left|S^f_{J-2,0}\ \cdots\right. \ \left. S^f_{J-2,2^{J-2}(-1)}\right\}^{\mathrm{T}} \\ \qquad\qquad\qquad\qquad\qquad\qquad \vdots \\ \mathbf{W}_{J-1}\oplus\mathbf{W}_{J-2}\oplus\mathbf{W}_{J-3}\oplus \qquad \cdots \qquad\qquad\qquad \oplus\mathbf{V}_{J-P}. \end{array}$$

Irrespective of the number of wavelet space decompositions, coefficients from the coarse scaling function space ($\mathbf{V}_{J-P}$) are always kept. This point will be exploited later when discussing the incorporation of boundary conditions.

An estimate for the number of operations involved during the transform algorithm can be obtained by noting that it requires $2(N-1)$ filter coefficients to define the primal scaling function $\phi(x)$ which spans $\mathbb{P}_N$ (the space of polynomials of degree $<N$). The part of the transform algorithm which calculates the wavelet coefficient $d^f_{j,k}$ for a given resolution j can be accomplished in $2(N-1)+1$ floating point operations. The subsampling process required for the scaling function coefficients $S^f_{j,k}$ requires a further 2^j operations. Overall, $2^{j+1}N$ operations are required per resolution j (this presupposes that the dimension of $\mathbf{W}_j$ is 2^j). For a given P passes of the transform algorithm, then, there are $2N\sum_{i=J-P}^{J} 2^i = 2^{J-P}N\{2^{P+1}-1\}$ operations. $\mathbf{V}_J$ represents the highest resolution in the discretisation. We note that in deriving this estimate, we have not assumed that the decomposition can continue until reaching $\mathbf{V}_0$. The reason for this stems from a minimal resolution requirement, which prevents the support of the boundary wavelets from overlapping. The minimal resolution argument is given for periodic Daubechies wavelets in [36] and can be readily adapted to the basis used here.

3.3. *Interval Construction*

We require at the outset that

$$\begin{aligned} \dim(\mathbf{V}_j) &= \dim(\mathbf{W}_j) + 1 \\ \dim(\tilde{\mathbf{V}}_j) &= \dim(\tilde{\mathbf{W}}_j) + 1. \end{aligned} \tag{27}$$

This stipulation leads to the bounding of the discretised interval by scaling functions which, in turn, allows simple incorporation of boundary conditions.

We let $\mathbf{V}_j$ denote a scaling function space, discretising [0, 1] into 2^j+1 elements. Each element is associated with a scaling function $\phi_{j,k}$, located such that $\phi_{j,k}(x_{j,m}) = \delta_{k,m}$, where $x_{j,m} = m2^{-j}$, $0 \le m, k \le 2^j$. We define similarly the wavelet space $\mathbf{W}_j$ to discretise [0, 1] into 2^j elements $\psi_{j,k}$, each of which satisfies $\psi_{j,k}(\tilde{x}_{j,m}) = \delta_{k,m}$, $\tilde{x}_{j,m} = x_{j+1,2m+1}$, $0 \le m \le 2^j - 1$, $0 \le k \le 2^j$. To maintain biorthonormality of the basis, it is necessary to modify $\phi_{j,k}(x)$ as and when the support of the function intersects a boundary. If we let $\phi^L_{j,k}(x)$, $\phi_{j,k}(x)$, and $\phi^R_{j,k}(x)$ denote the leftmost, central, and rightmost basis functions in a discretisation, respectively, it can be shown that [34]

$$\begin{aligned} \phi^L_{j,k}(x) &= \phi_{j,k}(x) + \sum_{m=0}^{N-1} e^L_{m,k}\phi_{j,-(m+1)}(x), \quad 0 \le k \le N-1 \\ \phi^R_{j,k}(x) &= \phi_{j,k}(x) + \sum_{m=0}^{N-1} e^R_{m,k}\phi_{j,m+2^j+1}(x), \quad 2^j - N + 1 \le k \le 2^j; \end{aligned} \tag{28}$$

$\underline{e}^L$ and $\underline{e}^R$ are matrices arising from the construction of the edge basis functions, and contain a finite number ($N \times N$) of nonzero entries. The limits on k appearing in Eq. (28) arise as a result of the compact support of $\phi(x)$. It is straightforward to demonstrate that in the regions where the scaling functions are modified to incorporate the edge of the domain,

the relations

$$\begin{aligned}\psi^L_{j,k}(x) &= \phi^L_{j+1,2k+1}(x),\\ \psi^R_{j,k}(x) &= \phi^R_{j+1,2k+1}(x)\end{aligned} \tag{29}$$

are applicable [28].

The interval construction of the wavelet basis modifies slightly the transform algorithm, in that the wavelet coefficients $d^f_{j,m}$ are now calculated from

$$d^f_{j,m} = S^f_{j+1,2m+1} - \sum_{n=0}^{2^j} \Gamma^b_{mn} S^f_{j,n} \tag{30}$$

with Γ^b_{mn} defined as

$$\Gamma^b_{mn} = \phi^{[]}\left\{m - n + \frac{1}{2}\right\}, \tag{31}$$

and $\phi^{[]}(x) = \phi^L(x)$, $\phi(x)$, or $\phi^R(x)$, depending on the indices m and n.

3.4. *Differentiation*

Differentiation of the wavelet expansion of a function leads to the transformed representation being "lifted" from the space onto which it was originally projected. In the context of orthogonal wavelet bases, Liandrat and Tchamitchian [37] have shown how a linear operator T may be approximated on a single scaling function space $\mathbf{V}_j$ by T_j, where

$$T_j = P_{\mathbf{V}_j} T P_{\mathbf{V}_j}. \tag{32}$$

Furthermore, they show that the causal property of the multiresolution analysis leads to a decomposition of T_j onto a hierarchy of wavelet spaces referred to as the *standard decomposition*. The standard decomposition has been adopted here for the calculation of the wavelet expansions of the derivatives appearing in the transport equations. The derivation of these decompositions in the context of the wavelet basis adopted here is novel and is further discussed in Appendix A.

4. SOLUTION STRATEGY

To demonstrate the strategy adopted by our proposed method, consider a generic transport equation for some scalar property ξ, defined over some interval $\Omega = [x_l, x_r]$:

$$\begin{aligned}\frac{\partial}{\partial t}\{\rho\xi\} &= -\frac{\partial}{\partial x}\{\rho u \xi\} + S^\xi + \frac{\partial}{\partial x}\left\{D^\xi \frac{\partial \xi}{\partial x}\right\}, && x \notin \partial\Omega,\\ \frac{\partial}{\partial t}\{\rho\xi\} &= -\chi^L(t), && x = x_l,\\ \frac{\partial}{\partial t}\{\rho\xi\} &= -\chi^R(t), && x = x_r.\end{aligned} \tag{33}$$

S^{ξ} represents a source term for ξ and D^{ξ} is a characteristic diffusivity. $\chi^{L}(t)$ and $\chi^{R}(t)$ are time-dependent boundary conditions for the left- and right-hand ends of the computational domain, respectively. For ease of exposition and for compatibility with the characteristic-based boundary treatment of Thompson [38], we omit the diffusive terms from the previous equations. Diffusive boundary conditions can be implemented in the same way as the characteristic boundary conditions we will now discuss. By allowing the incorporation of both inviscid, time-dependent, and viscous boundary conditions, our numerical scheme is fully compatible with the Navier–Stokes characteristic boundary condition (NSCBC) treatment of Poinsot and Lele [20] and of Baum *et al.* [39] for reactive systems.

We begin by stating that the numerical scheme is not applied to the governing equation as detailed above, but to its wavelet-transformed counterpart,

$$\frac{\partial}{\partial t}\left\{\mathcal{P}_{J-P}^{J-1}(\varrho\xi)\right\} = -\partial_{J}^{(1)}\{\rho u\xi\} + \mathcal{P}_{J-P}^{J-1}\{S^{\xi}\}, \quad x \notin \partial\Omega, \tag{34}$$

where $\mathcal{P}_{J-P}^{J-1} = (P_{\mathbf{V}_{J-P}} + \sum_{i=J-P}^{J-1} P_{\mathbf{W}_i})$ and $\partial_{J}^{(1)}$ is the standard decomposition of d/dx—defined here as $(\mathcal{P}_{J-P}^{J-1}(d/dx)\mathcal{P}_{J-P}^{J-1})$. The diffusion term has been omitted, in line with earlier comments. We observe that in using a multiresolution strategy to discretise the problem, we represent the domain $P+1$ times, where P is the number of different resolutions in the discretisation (P wavelet spaces and the coarse resolution scaling function space $\mathbf{V}_{J-P}$, $P \geq 1$). While in the transform domain, each representation of the solution (defined at some characteristic resolution resolution quantified by p) should be supplemented by boundary conditions of some form.

Examining, first, the boundary conditions applied to the coarse scaling function space $\mathbf{V}_{J-P}$, we first assume that the right-hand side of Eq. (34) has been calculated *without* boundary conditions and that the result of this calculation is expressed across the hierarchy of wavelet spaces and $\mathbf{V}_{J-P}$. We recall from Eqs. (21) and (26) that the set of scaling function coefficients for the right-hand side of Eq. (34) in $\mathbf{V}_{J-P}$—$\{S_{J-P}^{\rho\xi}\}$ (say)—verify $\{S_{J-P}^{\rho\xi}\} \subset \{S_{J-P+1}^{\rho\xi}\}$. Furthermore, $S_{J-P,0}^{\rho\xi} = S_{J,0}^{\rho\xi}$ and $S_{J-P,2^{J-P}}^{\rho\xi} = S_{J,2^{J}}^{\rho\xi}$, which are the physical space values of the right-hand side of Eq. (34) evaluated at the boundaries of the domain. Hence, the incorporation of boundary conditions into $\mathbf{V}_{J-P}$ involves simply replacing $S_{J-P,0}^{\rho\xi}$ by $-\chi^{L}(t)$ and $S_{J-P,2^{J-P}}^{\rho\xi}$ by $-\chi^{R}(t)$.

The wavelet space treatment is slightly more complicated. By examining Eq. (29), it is straightforward to demonstrate that $\mathrm{supp}\{\psi^{L}(x)\} \cap \partial\Omega = \{\emptyset\} = \mathrm{supp}\{\psi^{R}(x)\} \cap \partial\Omega$. Hence, there are no wavelets on the boundary, and no boundary conditions need be applied to them directly. However, the original wavelet coefficients for each of the $\mathbf{W}_i$ obtained from Eq. (34) were derived without the influence of $\chi^{L}(t)$ and $\chi^{R}(t)$. As $S_{J-P,0}^{\rho\xi}$ and $S_{J-P,2^{J-P}}^{\rho\xi}$ have been replaced by $-\chi^{L}(t)$ and $-\chi^{R}(t)$ at the boundaries, we must recalculate the values of the wavelet coefficients that are influenced by this modification.

Now, by definition, the wavelet coefficients for the right-hand side of Eq. (34) can be written

$$d_{i,m}^{\rho\xi} = S_{i+1,2m+1}^{\rho\xi} - \sum_{\eta=0}^{2^{i}} \Gamma_{m\eta} S_{i,\eta}^{\rho\xi}, \quad i = J-P, \ldots, J-1, \tag{35}$$

but, the first and last elements $S_{i,0}^{\rho\xi}$ and $S_{i,2^i}^{\rho\xi}$ are now equal to $-\chi^L(t)$ and $-\chi^R(t)$, respectively. Hence, Eq. (35) must be modified to

$$\left\{d_{i,m}^{\rho\xi}\right\}^b = S_{i+1,2m+1}^{\rho\xi} - \Gamma_{i,0}\chi^L(t) - \Gamma_{i,2^i}\chi^R(t) - \sum_{\eta=1}^{2^i-1}\Gamma_{m,\eta}s_{i,\eta}^{\rho\xi}, \quad i = J-P,\ldots,J-1. \tag{36}$$

Here, $\{\cdot\}^b$ is used to denote a boundary influenced quantity. By ensuring that the boundary basis functions from the left- and right-hand ends of the domain do not overlap, the appearances of $\chi^L(t)$ and $\chi^R(t)$ are mutually exclusive. By subtracting Eq. (35) from Eq. (36), we obtain

$$\left\{d_{i,m}^{\rho\xi}\right\}^b = d_{i,m}^{\rho\xi} + \Gamma_{i,0}\left\{S_{i,0}^{\rho\xi} - \chi^L(t)\right\} + \Gamma_{i,2^i}\left\{S_{i,2^i}^{\rho\xi} - \chi^R(t)\right\}, \quad i = J-P,\ldots,J-1. \tag{37}$$

The compact support of $\phi^{[]}(x)$, and the structure of $\phi^L(x)$ and $\phi^R(x)$ means that the boundary modification of Eq. (37) need only be applied to the first and last N coefficients of each of the expansions in $\mathbf{W}_i$, $i = J-P,\ldots,J-1$.

5. RESULTS

A code has been written which embodies the techniques discussed in earlier sections. The algorithm uses an $N = 4$ interpolating wavelet (shown in Fig. 1). Derivative approximations based on this wavelet have fourth-order accuracy [40]. The code requires as its input a set

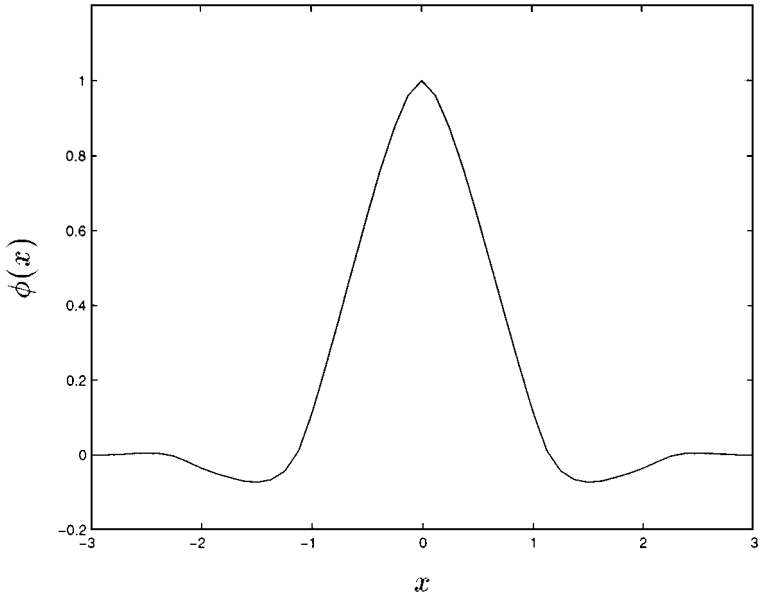

FIG. 1. $N = 4$ interpolating wavelet.

of initial estimated species mass fraction profiles, as well as estimated profiles for density, velocity, and temperature. The pressure and stagnation internal energy are determined from these initial data and subsequently all of the principal dependent variables are projected onto the hierarchy of wavelet spaces. The solution is time advanced in the transform domains until the end of the simulation is reached, returning to physical space only for the evaluation of reaction rate or inertial nonlinear terms. The time-dependent boundary conditions are imposed on the coarsely resolved scaling function space directly at each time step, and subsequently convolved onto each member of the wavelet spaces as discussed in the previous section. The time stepping algorithm adopted is that of Wray [41] and is a minimal storage Runge–Kutta method of third order. Transients arising from the approximate nature of the initial conditions are allowed to propagate out of the domain, and once a pseudo-stationary solution is obtained, the simulation is stopped.

To assess the comparative execution time of our proposed numerical method, the test problem was investigated a second time, employing a traditional numerical method. We chose a second-order centred differencing scheme, as this is a popular option for simple problems, and it is also one of the fastest available numerical algorithms. In direct comparison, the new wavelet scheme required 80% more time to execute than the explicit differencing scheme. This makes the scheme competitive with higher order traditional methods such as compact finite differencing schemes [20]. The principal penalties in the execution time of the proposed wavelet scheme arise from the evaluation of nonlinear terms (further discussed in [42]) and the compression and expansion of the transformed species mass fraction profiles.

Figure 2 demonstrates the implementation of the NSCBC boundary conditions and shows a pressure wave propagating toward a computational boundary. The fluid through which the wave is propagating is a quiescent mixture of stoichiometric methane and air, and the theoretical sound speed for such a mixture is 343.2 m/s. As seen in the figure, there is no appreciable reflection at the boundary and the simulated sound speed, at 343.1 m/s, is in excellent agreement with the theoretical one. The resolution for this calculation is 256 grid points (corresponding to $\mathbf{V}_8$), with a most coarsely resolved space of 32 nodes ($\mathbf{V}_{J-P} = \mathbf{V}_5$). For the acoustic perturbation shown, the profile is considerably overresolved when using a grid of 256 points. We adopted this resolution for two reasons. First, this was the resolution at which the structure of a flame based on the reduced methane mechanism was subsequently examined. Second (and more importantly), the resolution adopted contained a number of wavelet spaces and provided a significant test problem for the incorporation of the time-dependent boundary conditions discussed earlier.

For the four-step reduced methane mechanism, the nondimensionalisation of the governing equations has made use of the reference quantities

$$(C_p)_0 = 1067.07\,\mathrm{J\,kg^{-1}\,K^{-1}}, \quad T_0 = 300\,\mathrm{K}, \quad \rho_0 = 1.1219\,kg\,m^{-3} \tag{38}$$

$$\mathcal{R}^0 = 301.03\,\mathrm{J\,kg^{-1}\,K^{-1}} \quad W_0 = 1\,\mathrm{kg\,kmol^{-1}} \quad u_l^0 = 0.5\,\mathrm{m\,s^{-1}} \tag{39}$$

which lead to the dimensionless groups

$$\mathrm{Re} = 30, \quad \mathrm{Pr} = 0.7; \quad \mathcal{M}^2 = 0.19873 \times 10^{-5}.$$

The dimensionless parameters relating to the chemistry of the problem are given in Tables I, II, and III.

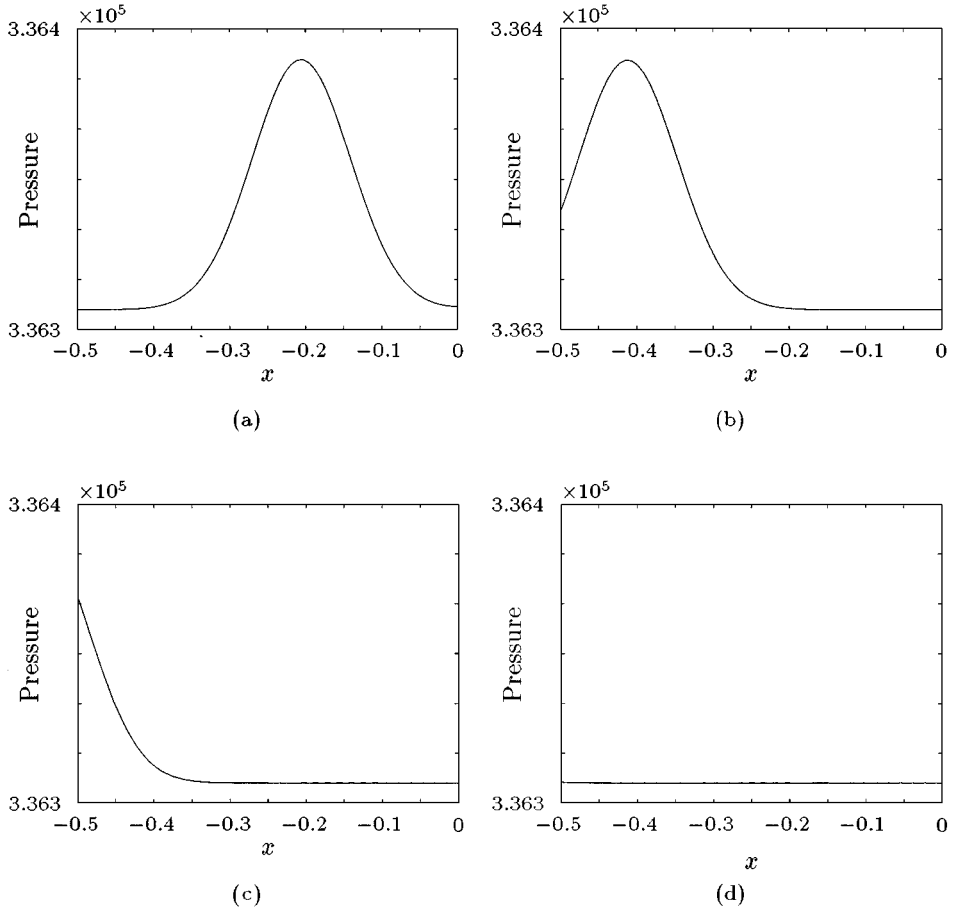

FIG. 2. Acoustic wave propagation across an NSCBC boundary condition.

Figures 3a–c show the species mass fraction profiles obtained from a quasi-steady simulation of the four-step-reduced mechanism stoichiometric methane–air flame. The quasi-steady nature of the solution was obtained by balancing the flame speed against the speed of the incoming reactants. The flame speed in one dimension can be obtained from the reaction rate profile of any of the species and is derived by integrating its species mass fraction transport equation over the domain. The range of the integration should be sufficiently large to ensure that the reaction rates are exponentially small at the limits. The rate of mass

TABLE I

Quantities Used in the Derivation of the Dimensionless Reaction Rates

k	$(B_i)_{\text{dim}}$	$(-\frac{E_i}{\mathcal{R}^0})_{\text{dim}}$	B_i	$(-\frac{E_i}{\mathcal{R}^0})$	α_i	n
1	2.0×10^{11}	−4401.2	4.5177×10^9	−14.77	0.0	2
5	2.3×10^{12}	372.84	6.1540×10^8	1.25	−0.8	3
10	4.4×10^3	0.0	5.1132×10^5	0.0	1.5	2
11	2.2×10^1	−8455.1	1.3152×10^7	−28.37	3.0	2

Note. The units in columns (2) and (3) are $(kmol/m^3)^{-(n-1)}s^{-1} \circ K^{-\alpha}$ and $\circ K$. All other quantities are dimensionless.

TABLE II
Molecular Transport Coefficients and Characteristic Gas Constants for Various Species

Species	Lewis number, Le	R_α
CH_4	0.97	0.487
CO	1.11	0.278
CO_2	1.39	0.177
H	0.18	0.390
H_2	0.3	0.433
H_2O	0.83	0.243
O_2	1.11	0.278

consumption of reactants is then

$$\rho_r u_r = \frac{\int w_\alpha \, dx}{(Y_\alpha)_o - (Y_\alpha)_i}, \tag{40}$$

where the suffices i and o refer to inlet and outlet conditions, respectively. It should be noted that this equation is valid only for pseudo-stationary solutions, and if this is not the case, a modification to incorporate time-dependent effects must be made. The flame speed has been evaluated using this method and has been found to be somewhat higher than the accepted value for this mixture under similar conditions of temperature and pressure. This tendency has also been observed in previous studies of premixed laminar flames using the same reduced reaction mechanism and is certainly *not* associated with the particular numerical method presented here.

Downstream of the flame, the temperature of the products is 6.8 dimensionless units, corresponding to 2040 K. This figure is in excellent agreement with [43] who have used more complex relations for the reaction rate terms.

Figures 4a–c show the reaction rate profiles for all species except N_2 (recall $w_{N_2} = 0$). We see that the regions of significant reaction occupy 0.1–0.2 dimensionless length units, corresponding to 0.25 mm–0.5 mm in the physical domain. The flame thickness is in reasonable agreement with Echekki and Chen [24], but too close a comparison should not be made as the latter work used reactants with a preheat temperature of 800 K.

The reaction rate profiles shown in Fig. 4 indicate that the entire reacting portion of the flame has been captured within the computational domain, and this view is strengthened by

TABLE III
Equilibrium Constants for Reduced Methane Reaction Mechanism

K	C	$(T_i)_{\text{dim}}$	T_i
3	0.216	7658	25.53
II	0.035	3652	12.17
IV	1.48	6133	20.44

Note. Column (3) has the units of $^\circ K$. All other quantities are dimensionless.

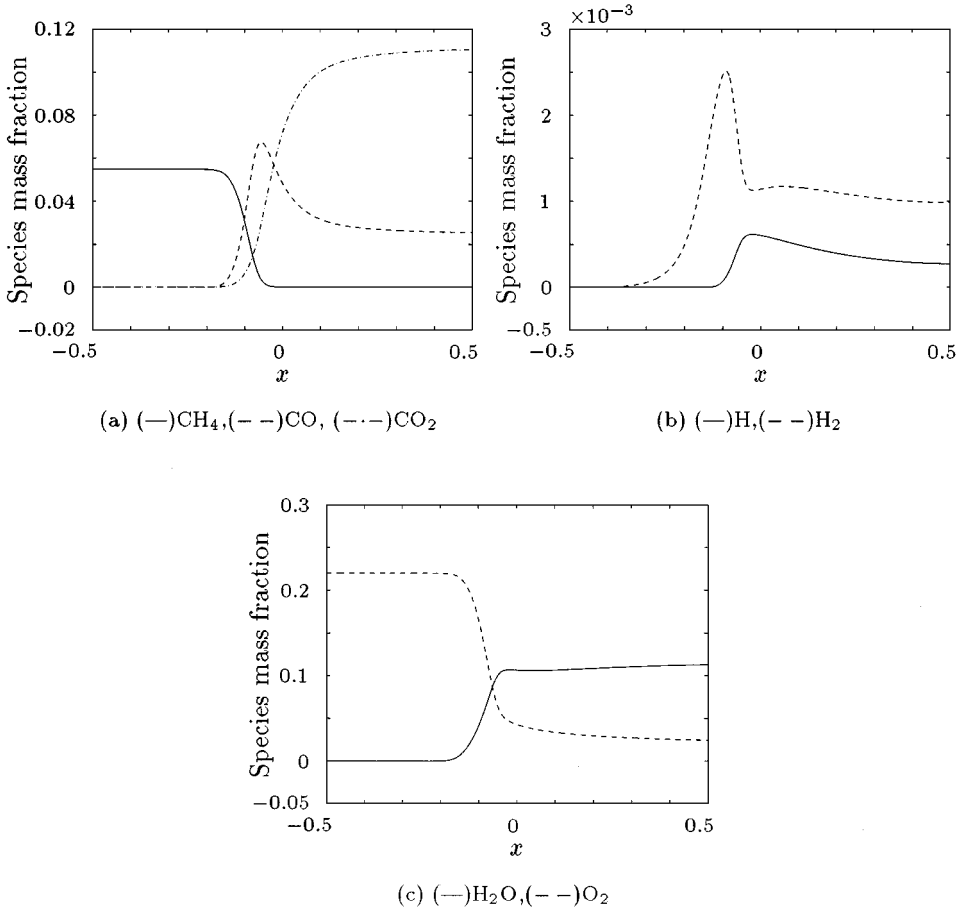

FIG. 3. Species mass fractions for stoichiometric premixed methane–air flame.

Fig. 5, which shows the enthalpy of the flow as a function of distance. We note that overall the flame is isenthalpic, as predicted by classical thermodynamic analyses.

Figure 6 shows the spatial distributions of temperature, density, velocity, and pressure. We see that there exists a significant pressure gradient within the reaction zone, but the global pressure drop across the flame remains small.

Thresholding. The principal advantage to solving the governing transport equations on the hierarchy of wavelet spaces lies in the sparsity of the transformed representation. When combustion occurs in the laminar flamelet regime, the species mass fraction profiles exhibit localised regions of large change within the flame structure, outside of which they are comparatively constant. The wavelet representation of such distributions can be exploited, as only those regions of rapid change are associated with wavelet coefficients of nontrivial magnitude.

The present adaptive scheme differs from those proposed by Vasiliev *et al.* [10–12] or Cai *et al.* [29, 30]. The adaptivity proposed in their work is most effective when there exists a few well-defined regions in the solution, where multiple scales are apparent. Our future goal is the investigation of turbulent combustion processes, where the space filling broad range of length scales apparent in the fully developed turbulence does not appear to

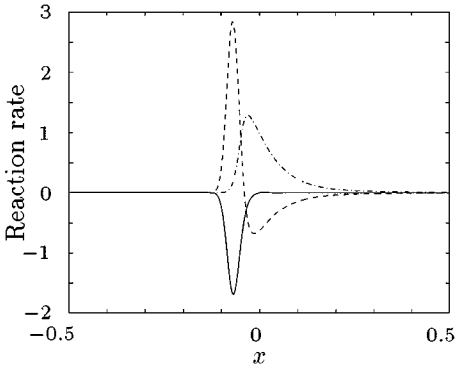

(a) (—)CH_4,(− −)CO, (−·−)CO_2

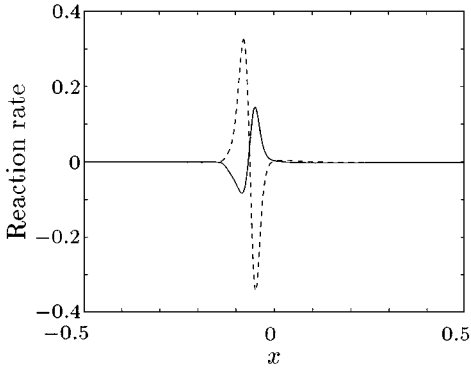

(b) (—)H,(− −)H_2

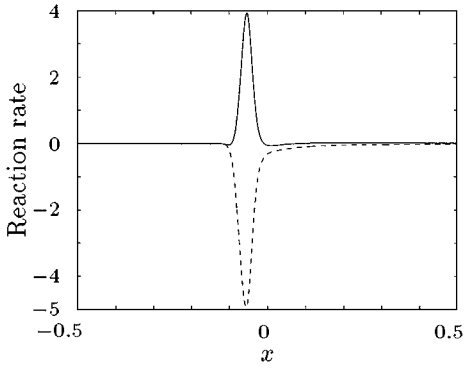

(c) (—)H_2O,(− −)O_2

FIG. 4. Species reaction rates for stoichiometric premixed methane–air flame.

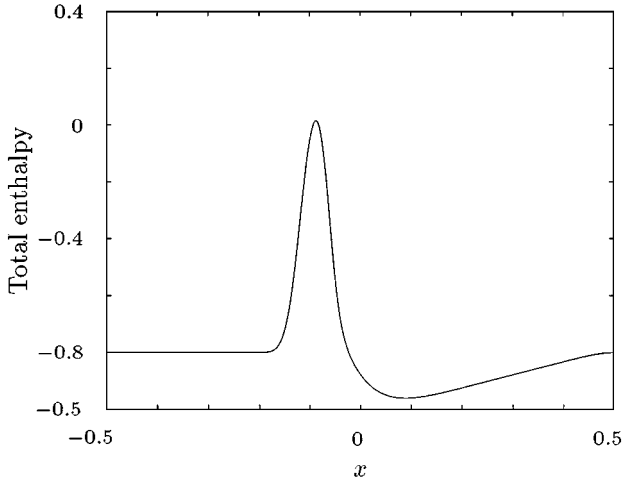

FIG. 5. Spatial distribution of total enthalpy for stoichiometric premixed methane–air flame.

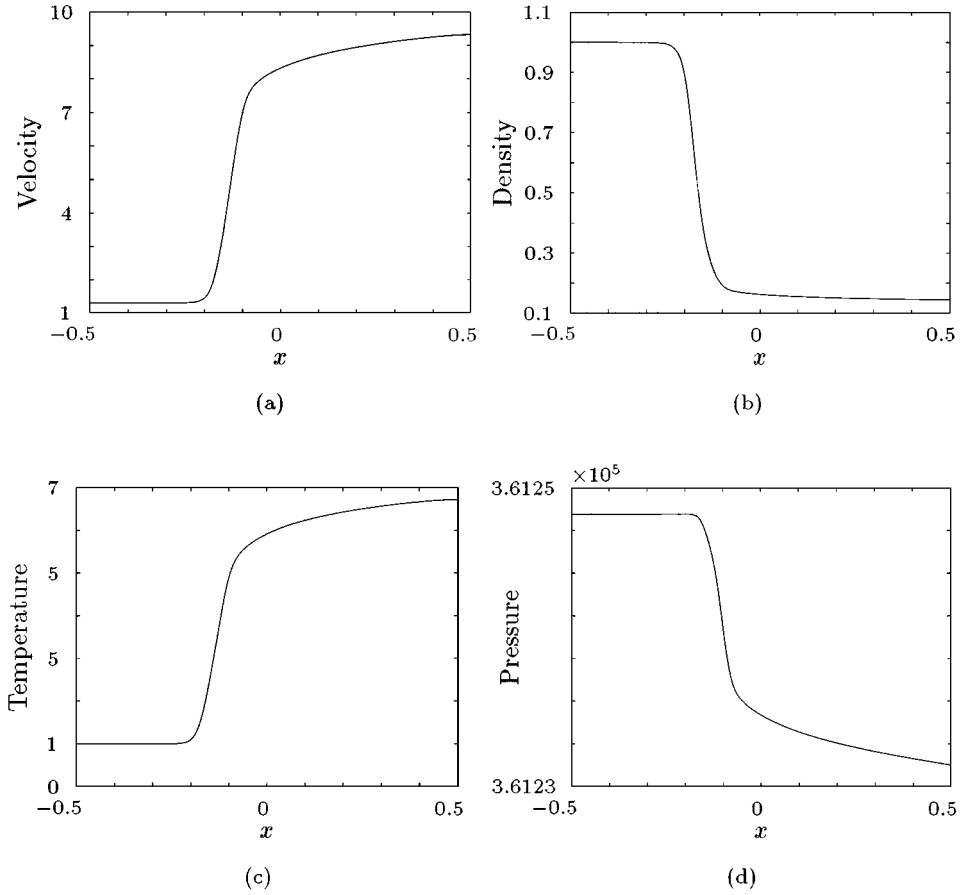

FIG. 6. Velocity, density, temperature, and pressure distributions associated with stoichiometric methane–air flame.

be well suited to treatment using adaptive techniques. We conclude that the discretisation of turbulent fluid flows using wavelets purely in their capacity for reducing information storage may not be the best approach.

The scale separation of the chemical kinetics is still significant in turbulent flows, however, and in particular, the species mass fraction of an element Y_α in regions of the flow with homogeneous chemical composition is undisturbed by turbulent fluctuations. By contrast, variations in Y_α close to the flame are large and highly localised. Hence, significant memory reductions may still be afforded by thresholding the wavelet expansions of each Y_α at some small finite value. Introducing this technique for the species mass fractions but not the fluid flow variables would be cumbersome were it not possible to express the solution, equations, and boundary conditions in terms of their respective wavelet expansions. Furthermore, by applying the differential operators and time stepping techniques only to those regions where significant wavelet coefficients exist, considerable computational savings can be made.

Thresholding must be applied carefully, however. In reacting flows with complex chemistry, the equilibrium structure of the system may contain radical species whose concentrations are very small. It is important to avoid setting thresholding levels which result in

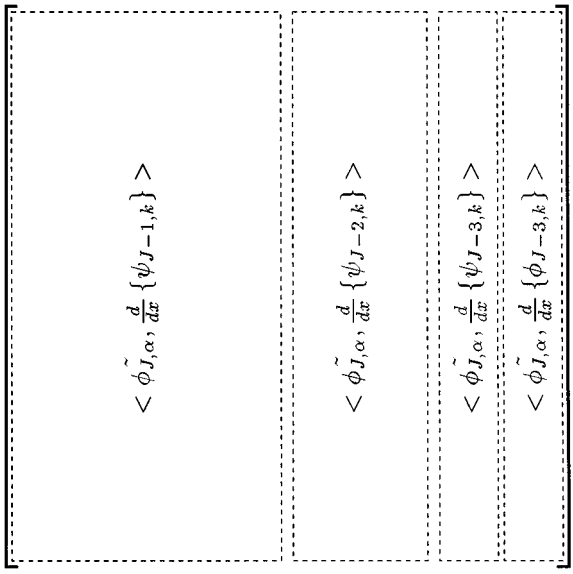

FIG. 7. Intermediate assembly of matrices during the construction of the nonstandard decomposition (four subspace decomposition).

the removal of such trace species, as this can have a disproportionately large effect on the nature of the flow.

Two remedies exist to deal with this problem. If thresholding is applied to the entire transform vector *including* $\mathbf{V}_{J-P}$, then the threshold level must be set below the equilibrium value of the species. This approach is undesirable in that we may not know the equilibrium composition of the flow, and if the equilibrium concentration of the species is small, the associated small threshold level leads to poor performance in the memory-saving algorithm.

The second approach is to apply the thresholding only to those components in the wavelet spaces. By retaining the coarse grained structure of the solution on $\mathbf{V}_{J-P}$, we are guaranteed to retain the crucial equilibrium structure of the flow. For this paper, we have adopted the first of these approaches. Not only is it straightforward to implement, but also represents the worst-case performance of the memory compression algorithm. Tables IV, V, and VI

TABLE IV
Variation of Solution Quality and Computer Memory Reduction with Wavelet Threshold Parameter (ϵ)

ϵ	Reduction	$\frac{\|(Y_H)-(Y_H)_\epsilon\|_2}{\|Y_H\|_2}$	$\frac{\|u-u_\epsilon\|_2}{\|u\|_2}$
0	—	0	0
10^{-8}	2.0358 : 1	9.0625×10^{-4}	1.0903×10^{-4}
10^{-7}	2.7788 : 1	2.4767×10^{-3}	4.1158×10^{-4}
10^{-6}	3.6377 : 1	1.7915×10^{-2}	6.4455×10^{-3}
10^{-5}	4.4618 : 1	6.6130×10^{-2}	5.3950×10^{-2}

Note. The suffix ϵ denotes a thresholded quantity. $\|u\|_2 = 1.1426 \times 10^2$, $\|Y_H\|_2 = 4.7908 \times 10^{-3}$, $\mathbf{V}_J = \mathbf{V}_8$, $\mathbf{V}_{J-P} = \mathbf{V}_6$.

TABLE V
Variation of Solution Quality and Computer Memory Reduction with Wavelet Threshold Parameter (ϵ)

ϵ	Reduction	$\frac{\|(Y_H) - (Y_H)_\epsilon\|_2}{\|Y_H\|_2}$	$\frac{\|u - u_\epsilon\|_2}{\|u\|_2}$
0	—	0	0
10^{-8}	2.2334 : 1	9.8208×10^{-4}	1.2016×10^{-4}
10^{-7}	3.2000 : 1	7.3761×10^{-3}	1.7680×10^{-3}
10^{-6}	4.7080 : 1	3.8448×10^{-2}	9.7572×10^{-3}
10^{-5}	6.5852 : 1	1.2507×10^{-1}	1.2409×10^{-2}

Note. The suffix ϵ denotes a thresholded quantity. $\|u\|_2 = 1.1426 \times 10^2$, $\|Y_H\|_2 = 4.7908 \times 10^{-3}$, $\mathbf{V}_J = \mathbf{V}_8$, $\mathbf{V}_{J-P} = \mathbf{V}_5$.

show by how much the memory required to resolve the chemical species reduces with increasing wavelet threshold. In each case, a uniform threshold was applied to all of the chemical species, and no further "tuning" of these parameters took place. It is worthwhile emphasising that when the threshold level is set to 10^{-5}, it is possible to resolve all eight species using less memory than that required to capture the single *reaction progress variable* [3, 14–16] of the much simplified single step chemical mechanism using more traditional numerical methods.

The sensitivity of the solution to an increasing absolute wavelet thresholding parameter is demonstrated in columns 3 and 4 of Table IV. The normalised l^2 error norms for velocity and radical hydrogen mass fraction are presented because empirical evidence suggests these are the most sensitive variables. Errors arising from *all* species mass fractions feed through to the velocity field via the pressure terms in the momentum equation and the thermal equation of state. Furthermore, the low Mach number of the flow renders the pressure particularly sensitive to perturbations (this is apparent from the Mach number divisor appearing in the dimensionless thermal equation of state—Eq. (5)).

Similarly, numerical evidence and examination of the reduced four-step chemical reaction mechanism reveals the crucial role played by the hydrogen radical. Without its presence, the reaction stops. As the species appears in very small quantities, it follows that small errors will produce a disproportionately large effect.

TABLE VI
Variation of Solution Quality and Computer Memory Reductions with Wavelet Threshold Parameter (ϵ)

ϵ	Reduction	$\frac{\|(Y_H) - (Y_H)_\epsilon\|_2}{\|Y_H\|_2}$	$\frac{\|u - u_\epsilon\|_2}{\|u\|_2}$
0	—	0	0
10^{-8}	2.3540 : 1	1.7554×10^{-3}	2.6214×10^{-3}
10^{-7}	3.4020 : 1	7.3815×10^{-3}	3.2328×10^{-3}
10^{-6}	5.1980 : 1	5.3998×10^{-2}	1.1872×10^{-2}
10^{-5}	8.1270 : 1	1.4897×10^{-1}	2.0886×10^{-2}

Note. The suffix ϵ denotes a thresholded quantity. $\|u\|_2 = 1.1426 \times 10^2$, $\|Y_H\|_2 = 4.7908 \times 10^{-3}$, $\mathbf{V}_J = \mathbf{V}_8$, $\mathbf{V}_{J-P} = \mathbf{V}_4$.

Despite the sensitivity of these quantities, we see that in general the errors arising as a result of thresholding are very small. It is clear from the results that the "selectiveness" of the wavelet thresholding is both robust and effective.

6. CONCLUSIONS

A new numerical scheme has been proposed based on a collocation-like strategy and making use of interpolating biorthogonal wavelet systems. The flexibility of the basis functions has been exploited to pave the way for an elegant treatment of general boundary conditions relevant to compressible fluid flow problems. The technique has been applied to a one-dimensional premixed laminar flame problem with a reduced four-step methane–air reaction mechanism. The spatial localisation of the flame structure leads to considerable sparsity in the wavelet representation of the species mass fraction distributions. This sparsity has, in turn, led to significant reductions in the memory required to resolve the problem accurately.

The reduction in memory required to resolve chemically active systems implies that simulations of much greater complexity can now be undertaken with little or no extra cost over those presently achievable. Future work will seek to improve the execution time of the algorithm by examining the evaluation of nonlinear terms while the solution remains in the transform domains.

APPENDIX A: DERIVATIVES IN INTERPOLATING (SECOND GENERATION) BIORTHOGONAL WAVELET SYSTEMS

For our scheme, we have adopted the standard decomposition [44] for the discretisation of the first and second derivatives. Define $\partial_J^{(n)}$ such that

$$\partial_J^{(n)}\{f(x)\} = P_{\mathbf{V}_J}\frac{d^n}{dx^n}\left\{P_{\mathbf{V}_J}(f(x))\right\}, \tag{41}$$

noting in passing that this expression only has meaning if the underlying basis functions have sufficient differentiability. Repeated application of the causal relation (Eq. (13)) leads to the standard decomposition

$$\partial_J^{(n)}\{f(x)\} = \left\{P_{\mathbf{V}_{J-P}} + \sum_{i=J-P}^{J-1} P_{\mathbf{W}_i}\right\}\frac{d^n}{dx^n}\left\{P_{\mathbf{V}_{J-P}} + \sum_{i=J-P}^{J-1} P_{\mathbf{W}_i}\right\}(f(x)). \tag{42}$$

Explicit calculation of the standard decomposition leads to the characteristic "starburst" structure in the operator, as depicted in [8].

To calculate explicitly the standard decomposition using the interpolating wavelets, we must first assemble the intermediate structure shown in Fig. 7. For this illustrative example, we work with the first derivative and use only $3+1$ approximation spaces. Each of the matrices in the assembly are of dimension $2^J \times 2^{J-i}$, where i can take any value between 1 and P. We denote by $\epsilon_{\alpha,k}^{J,J-i}$ a typical member of this assembly and define it as

$$\epsilon_{\alpha,k}^{J,J-i} = \int_0^1 \tilde{\phi}_{J,\alpha}\frac{d}{dx}\left\{\psi_{J-i,k}^{[]}\right\}dx. \tag{43}$$

where $\psi^{[]}_{J-i,k}(x)$ is [28]

$$\psi^{[]}_{J-i,k}(x) = \phi^{[]}_{J-i+1,2k+1}(x).$$

Recalling the definition of the primal wavelet and dual scaling function, Eq. (43) can be simplified to

$$\epsilon^{J,J-i}_{\alpha,k} = 2^{J-i+1}\phi^{[]'}(2^{-i+1}\alpha - 2k - 1), \tag{44}$$

where $\phi^{[]'}$ denotes the derivative of $\phi^{[]}$. The problem we now face is that of calculating the values of the primal scaling function at rational dyadic grid points. Differentiating equation (24), we find

$$\frac{d}{dx}\{\phi(x)\} = 2\sum_{\xi\in\mathbb{Z}} \phi\left\{\frac{\xi}{2}\right\}\frac{d}{dx}\{\phi(2x-\xi)\}. \tag{45}$$

Defining $h_\xi = \phi(\xi/2)$, Eq. (43) is identical to the two-scale relation given by Beylkin [45] in his discussion of derivative expansions in orthogonal wavelet bases. The procedures described in that paper can be directly applied to calculate the required derivative values for our wavelet system. After the values of $(d/dx)(\phi(x))$ are calculated at all integer nodes, Eq. (45) can be applied recursively to calculate the values of $(d/dx)(\phi(x))$ at any required dyadic point.

After calculation of the assembly of submatrices $\epsilon^{J,J-i}_{\alpha,k}$, the full standard decomposition is determined by applying the standard transform (i.e. Eqs. (23) and (26)) to the columns of the assembled matrix. The accuracy of the approximation for the $N = 4$ case is formally fourth order. A discussion on the construction, accuracy, and stability of the derivative approximations obtained using interpolating wavelets with different values of N is presented in [40].

APPENDIX B: NOMENCLATURE

x	spatial coordinate, $x_{j,k} = 2^{-j}k$	t	time
ρ	density	u	x directed velocity
P	pressure	E	stagnation internal energy
T	temperature	Y	species mass fraction
q	heat flux vector	ω	reaction rate
$\mathcal{D}$	binary diffusivity	μ	viscosity
λ	thermal conductivity	$\mathcal{M}$	Mach number
γ	adiabatic index	Re	Reynolds number
Sc	Schmidt number	Pr	Prandtl number
Le	Lewis number	$\mathbb{Z}$	the set of integers
$\mathbb{R}$	the set of reals	$\mathcal{R}^0$	universal gas constant
R	characteristic gas constant	W	molar mass
N	polynomial span of primal scaling function		

Suffices

o	reference quantities
α	chemical species

ACKNOWLEDGMENTS

Financial support for this work was provided by EPSRC.

REFERENCES

1. S. Corrsin, Turbulent flow, *Am. Sci.* **49**, 300 (1961).
2. P. A. Libby and K. N. C. Bray, Implications of the laminar flamelet model in premixed turbulent combustion, *Combust. Flame* **39**, 33 (1980).
3. K. N. C. Bray, P. A. Libby, and J. B. Moss, Unified modeling approach for premixed turbulent combustion. Part 1. General formulation, *Combust. Flame* **61**, 87 (1985).
4. J. Frölich and K. Schneider, An adaptive wavelet-vaguelette algorithm for the solution of PDEs, *J. Comput. Phys.* **130**, 174 (1997).
5. J. Frölich and K. Schneider, A fast algorithm for lacunary wavelet bases related to the solution of PDEs. *C.R. Math. Rep. Acad. Sci. Canada* **16**, 83 (1996).
6. H. Bockhorn, J. Frölich, and K. Schneider, An adaptive two-dimensional wavelet-vaguelette algorithm for the computation of flame balls, technical report, Universität Kaiserslautern, 1995.
7. J. Frölich and K. Schneider, Numerical simulation of decaying turbulence in an adapted wavelet basis, *Appl. Comput. Harm. Anal.* **2**, 393 (1995).
8. E. Bacry, S. G. Mallat, and G. Papanicolaou, A wavelet based space-time adaptive numerical method for partial differential equations, *Math. Modelling Numer. Anal.* **26**(7), 793 (1992).
9. B. L. Bihari, Multiresolution schemes for conservation laws with viscosity, *J. Comput. Phys.* **123**, 207 (1996).
10. O. V. Vasilyev, S. Paolucci, and M. Sen, A multilevel wavelet collocation method for solving partial differential equations in a finite domain, *J. Comput. Phys.* **120**, 33 (1995).
11. O. V. Vasilyev and S. Paolucci, A dynamically adaptive multilevel wavelet collocation method for solving partial differential equations in a finite domain, *J. Comput. Phys.* **125**, 498 (1996).
12. O. V. Vasilyev and S. Paolucci, A fast adaptive wavelet collocation algorithm for multidimensional PDEs, *J. Comput. Phys*, **138**, 16 (1997).
13. P. A. Libby and F. A. Williams (Eds.), *Turbulent Reacting Flows*. (Academic Press, New York, 1994).
14. K. N. C. Bray and J. B. Moss, *A Unified Statistical Model of the Premixed Turbulent Flame*, Technical Report AASU 335, University of Southampton, 1974.
15. K. N. C. Bray and J. B. Moss, A unified statistical model of the premixed turbulent flame, *Acta Astronaut.* **4**, 291 (1977).
16. R. S. Cant and K. N. C. Bray, A theoretical model of premixed turbulent combustion in closed vessels, *Combust. Flame* **76**, 243 (1989).
17. F. A. Williams, *Combustion Theory*, 2nd ed. (Addison Wesley, Menlo Park, CA, 1985).
18. *Applications of Direct and Large Eddy Simulation to Transition and Turbulence*, No. AGARD-CP-551, Neuilly-Sur-Seine, France, 1994.
19. J. D. Buckmaster and G. S. S. Ludford, *Theory of Laminar Flames* (Cambridge Univ. Press, Cambridge, 1982).
20. T. J. Poinsot and S. K. Lele, Boundary conditions for direct simulations of compressible viscous flows, *J. Comput. Phys.* **101**, 104 (1992).
21. R. J. Kee and F. M. Rupley, *Chemkin II: A FORTRAN Chemical Kinetics Package for the Analysis of Gas-Phase Chemical Kinetics.* Technical Report SAND89-8009, Sandia National Laboratories, Livermore, CA 94551, 1989.
22. K. K. Kuo, *Principles of Combustion* (Wiley, New York, 1986).
23. N. Peters and F. A. Williams, The asymptotic structure of stoichiometric methane–air flames, *Combust. Flame* **68**, 185 (1987).
24. T. Echekki and J. H. Chen, Unsteady strain rate and curvature effects in turbulent premixed methane–air flames, *Combust. Flame* **106**, 184 (1996).

25. A. Cohen, I. Daubechies, and J. C. Feauveau, Biorthogonal bases of compactly supported wavelets, *Commun. Pure Appl. Math.* **45**, 485 (1992).
26. A. Cohen, I. Daubechies, and P. Vial, Wavelets on the interval and fast wavelet transforms, *Appl. Comput. Harmonic Anal.* **1**, 54 (1993).
27. P. Monasse and V. Perrier, Orthonormal wavelet bases adapted for partial differential equations with boundary conditions, *SIAM J. Math. Anal.* **28**, 1040 (1998).
28. R. Prosser, *Numerical Methods for the Computation of Combustion*, Ph.D. thesis, Cambridge University, 1997.
29. W. Cai and J. Wang, Adaptive multiresolution collocation methods for initial boundary value problems of nonlinear PDEs, *SIAM J. Numer. Anal.* **33**, 937 (1996).
30. W. Cai and W. Zhang, An adaptive spline wavelet ADI (SW-ADI) method for two-dimensional reaction–diffusion equations, *J. Comput. Phys.* **139**, 92 (1998).
31. W. Sweldens, The lifting scheme: A custom design construction of biorthogonal wavelets, *Appl. Comput. Harm. Anal.* **3**, 186 (1996).
32. W. Sweldens, The lifting scheme: A construction of second generation wavelets, *SIAM J. Math. Anal.* **29**, 511 (1997).
33. P. Schröder and W. Sweldens, Building your own wavelets at home, in *ACM SIGGRAPH Course Notes*, 1996.
34. D. L. Donoho, Interpolating wavelet transforms, in *NATO Advanced Study Institute Conference on "Wavelets and Applications," Il Ciocco, Italy, August 1992.*
35. G. Deslauriers and S. Dubuc, Symmetric iterative interpolation processes, *Constr. Approx.* **5**, 49 (1989).
36. J. M. Restrepo, G. K. Leaf, and G. Schlossnagle, *Periodized Daubechies Wavelets*, Technical Report MCS-P423-0394, Mathematics and Computer Science Division, Argonne National Lab., Illinois, 1994. [http://www.mathsoft.com/wavelet.html]
37. J. Liandrat and Ph. Tchamitchian, *Resolution of the 1-D Regularised Burgers Equation using a Spatial Wavelet Approximation*, Technical Report 90-83, NASA, ICASE Report, December 1990.
38. K. W. Thompson, Time dependent boundary conditions for hyperbolic systems, *J. Comput. Phys.* **68**, 1 (1987).
39. M. Baum, T. J. Poinsot, and D. Thévenin, Accurate boundary conditions for multicomponent reactive flows, *J. Comput. Phys.* **116**, 247 (1994).
40. R. Prosser and R. S. Cant, Differentiation using second generation wavelets, in preparation.
41. A. A. Wray, *Minimal Storage Time-Advancement Schemes for Spectral Methods* (NASA Research Center, Ames, IA, 1990).
42. R. Prosser and R. S. Cant, Nonlinearities and second generation wavelets, in preparation.
43. N. Peters and B. Rogg (Eds.), *Reduced Kinetic Mechanisms for Applications in Combustion Systems*, Lecture Notes in Physics, Vol. 15 (Springer-Verlag, Berlin, 1993).
44. G. Beylkin, R. Coifman, and V. Rokhlin, Fast wavelet transforms and numerical algorithms I, *Commun. Pure Appl. Math.* **44**, 141 (1991).
45. G. Beylkin, On the representation of operators in bases of compactly supported wavelets, *SIAM J. Numer. Anal.* **6**, 1716 (1992).